

High-Performance Color-Tunable Perovskite Light Emitting Devices through Structural Modulation from Bulk to Layered Film

Ziming Chen, Chongyang Zhang, Xiao-Fang Jiang, Meiyue Liu, Ruoxi Xia, Tingting Shi, Dongcheng Chen, Qifan Xue, Yu-Jun Zhao, Shijian Su, Hin-Lap Yip,* and Yong Cao

Hybrid organic–inorganic perovskite materials have attracted significant attention over the past few years owing to their advanced optoelectronic properties.^[1–5] Based on the strategies of interfacial, composition, and process engineering,^[6–10] solar cells based on these materials had been extensively studied and the efficiency rapidly reached over 20% nowadays.^[11–13] Recently, photoluminescence (PL) and electroluminescence (EL) of hybrid perovskite materials were also studied and it was found that the optical properties of perovskites can be tuned either by varying their compositions or nanostructures.^[14–23] Perovskites with wide range of emission spectrum had been achieved by simply tuning the ratio of halide ions in $\text{CH}_3\text{NH}_3\text{PbX}_3$ ($X = \text{I}, \text{Cl}, \text{Br}$).^[24–28] With their sharp emission peak and color-tunable properties, organic–inorganic hybrid perovskites are also considered as a promising candidate for lasing and light emitting applications.^[29–37] Efficient green and red emitting perovskite light emitting devices (LEDs) were reported by carefully controlling the charge injection and recombination in the perovskite layer.^[1,2,14,26,28,33] However, it remains difficult in achieving blue emitting LEDs based on $\text{CH}_3\text{NH}_3\text{PbCl}_3$ system because of its poor device stability, and the low solubility of the precursor materials in common solvents also makes it difficult to prepare smooth films for device testing. In addition to the bulk films, layered hybrid perovskite composed of alternating layers of small organic molecules and 2D perovskite sheets can be another promising system for light emitting application. The bandgap of layered perovskite can be easily tuned by controlling the number of perovskite unit within the layer structure.^[18] The charge recombination property of the layered perovskite can also be tuned as the introduction of organic molecules will decrease the overall dielectric constant of the hybrid film, which increases

the exciton binding energy and may facilitate more efficient radiative recombination in the hybrid film. Indeed, LEDs based on layered perovskites were demonstrated about two decades ago despite at that time the performance is very low and light emission was only observed under low temperatures.^[38–41] Recently, Lee et al. reported that through mixing layered and bulk perovskite, perovskite LEDs could achieve a high current efficiency (CE) of 4.9 cd A^{-1} .^[42] Jin et al. reported an $n = 1$ layered perovskite LED with violet emission despite a relatively low performance was reported.^[43] Moreover, Sargent et al. reported a high-performance layered perovskite LED achieving external quantum efficiency (EQE) of 8.8% with near-infrared emission based on the energy funneling effect.^[44]

In this work we systematically studied the structural change of $\text{CH}_3\text{NH}_3\text{PbBr}_3$ from bulk film to layered perovskite film and established structure-property relationship of the hybrid perovskite system. The different perovskite films were then applied as emissive layer to fabricate perovskite LEDs. We found that the device performance is strongly dependent on the perovskite film structure, and efficient and relatively stable blue and green LEDs were demonstrated under optimized structures. The $\text{CH}_3\text{NH}_3\text{PbBr}_3$ perovskite structure was tuned by adding different amount of 2-phenoxyethylamine (POEA), which molecular structure is shown in **Figure 1**, into $\text{CH}_3\text{NH}_3\text{PbBr}_3$ precursor solution. The final structure of the hybrid perovskite was mainly determined by two factors, including 1) the molecular interactions and 2) molecular ratio between the added molecule and the perovskite crystal. It is well known that the amine head group of small molecule can interact with the surface of perovskite by substitution of the surface CH_3NH_3^+ ion, while the different intermolecular interactions between the end groups of the molecules dictated the final structure of the hybrid perovskite. In the case of POEA, the benzene end groups interact through π – π stacking and lead to preferential directional growth of the perovskite crystal when the loading amount of molecules is small, while upon increasing the molecule loading, formation of layered perovskite structure were observed. The transition from bulk film to layered structure resulted in a drastic change in PL and EL of the $\text{CH}_3\text{NH}_3\text{PbBr}_3$ with emission color shifted from green to blue and the associated LED device performance improved extraordinarily at optimized conditions. Based on this strategy, our LED devices reached maximum EQE of 2.82% and CE of 8.23 cd A^{-1} . Also, we successfully fabricated perovskite layered-structure LEDs with green to blue EL in room temperature, which previously could be achieved at ultra-low temperature.^[38–41]

Z.-M. Chen, C.-Y. Zhang, Dr. X.-F. Jiang, M.-Y. Liu, R.-X. Xia, Dr. T.-T. Shi, Dr. D.-C. Chen, Q.-F. Xue, Prof. S.-J. Su, Prof. H.-L. Yip, Prof. Y. Cao
State Key Laboratory of Luminescent Materials and Devices
Institute of Polymer Optoelectronic
Materials and Devices
School of Materials Science and Engineering
South China University of Technology
381 Wushan Road, Guangzhou 510640, P. R. China
E-mail: msangusyip@scut.edu.cn



Prof. Y.-J. Zhao
Department of Physics
South China University of Technology
381 Wushan Road, Guangzhou 510640, P. R. China

DOI: 10.1002/adma.201603157

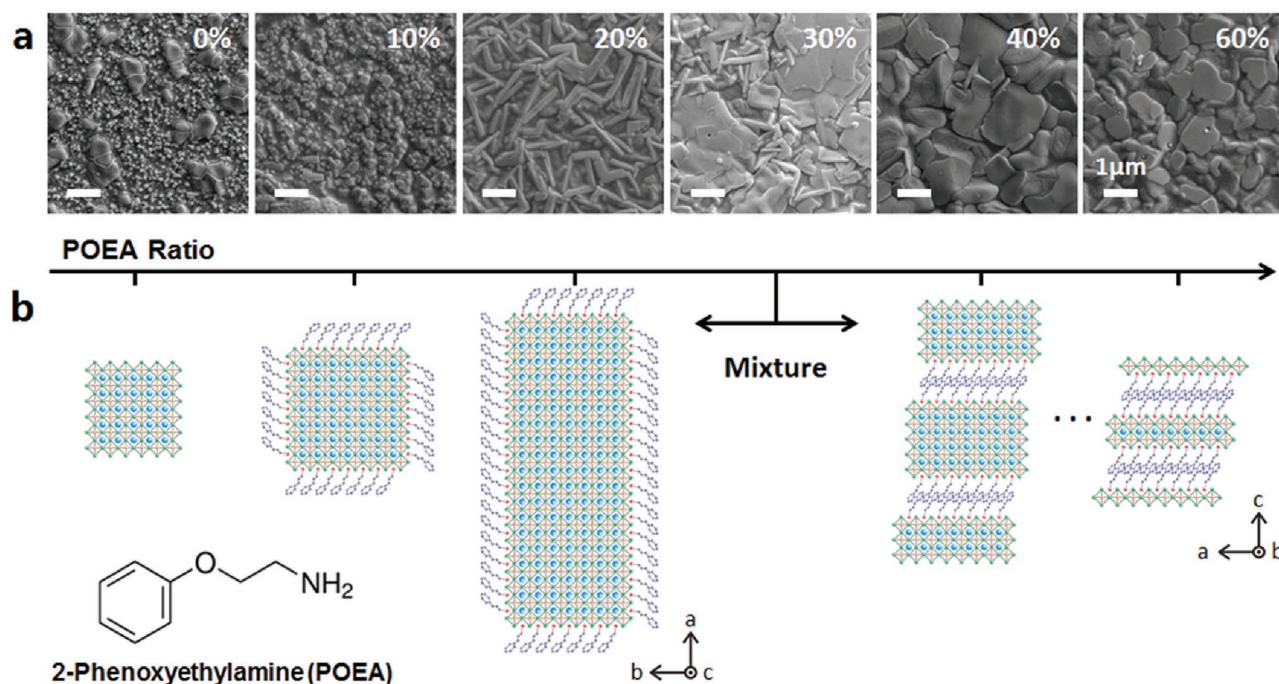


Figure 1. a) SEM image of perovskite films fabricated from $\text{CH}_3\text{NH}_3\text{PbBr}_3$ precursor solutions with different ratio of POEA. b) Schematic diagram of structural change of perovskite from bulk film to layered structure upon increasing POEA doping concentration.

Figure 1a shows the scanning electron microscopy (SEM) images of the perovskite films formed by the $\text{CH}_3\text{NH}_3\text{PbBr}_3$ precursor solutions added with different ratio of POEA. Figure 1b is a schematic diagram illustrating the corresponding structure changes from bulk to layered perovskite structure with increasing POEA concentration. A fixed molar ratio of methylammonium bromide (MABr): lead bromide (PbBr_2) = 3:1 was used to prepare the $\text{CH}_3\text{NH}_3\text{PbBr}_3$ precursor solutions. The SEM image of the pristine film shows that the film was composed of both small cubic perovskite crystals with grain size <100 nm and also some large aggregated domains with irregular shapes. The large aggregated domains were identified as MABr-rich phase due to the excess MABr in the precursor, which was verified by the X-ray diffraction (XRD) pattern in Figure 2a and energy dispersive X-ray spectroscopy (EDS) data in Figure S1 (Supporting Information). When the POEA ratio increased to 10%, the resultant film composed of $\text{CH}_3\text{NH}_3\text{PbBr}_3$ crystals with larger sizes (>200 nm) and less MABr-rich domains remained in the film. In this case, the POEA strongly interacted with the surface of $\text{CH}_3\text{NH}_3\text{PbBr}_3$ and generated a templating effect that promotes the growth of $\text{CH}_3\text{NH}_3\text{PbBr}_3$ into larger crystals. We also speculate that the introduction of POEA into the precursor solution may accelerate the decomposition of MABr to CH_3NH_2 (gas) and HBr (gas) and resulted in the formation of a purer and more uniform $\text{CH}_3\text{NH}_3\text{PbBr}_3$ phase as observed by the XRD study (detail discussion about the effect of POEA on the precursor solution is available in the Supporting Information). Increasing the POEA ratio to 20% started to result in one-dimensional growth of the $\text{CH}_3\text{NH}_3\text{PbBr}_3$ crystal into rod-like structure as shown in Figure 1a. The 1D growth of the perovskite crystal was facilitated by the strong interactions between the POEA

molecules when the doping concentration increased. Indeed, similar effect is commonly observed during the synthesis of nanostructured materials, in which ligands are added to template crystal growth into different shapes and dimensions.^[45] It is also worth to note that the $\text{CH}_3\text{NH}_3\text{PbBr}_3$ phase is quite pure with no observation of MABr peak from the XRD study, further suggesting that the POEA may help to suppress the undesired MABr formation. While further increasing the loading concentration of POEA to 30%, the film contained two different phases including the rod-like bulk crystals we observed in the 20% loading case and also some plate-like crystals with large grain, which are assigned as the layered perovskites evidenced by the appearance of new XRD peak at small 2θ angle of 2.902° and corresponds to a $d_{(100)}$ value of 30.42 \AA (labeled as A in Figure 2a).^[46,47] The formation of layered structure was driven by the high concentration of POEA, which enables the molecule to intercalate into the perovskite lattice and form the alternating POEA/perovskite layered structure.

The chemical formula of layered organic-inorganic hybrid perovskite is well established, which is represented as $(\text{POEA})_2(\text{MA})_{n-1}\text{Pb}_n\text{Br}_{3n+1}$ in our case in which n is the layer value.^[48] When a high concentration of POEA above 40% was added, only layered structures were formed, which was revealed by the absence of MAPbBr_3 peak from the XRD study. Instead, there are multiple XRD peaks labeled as A, B, C and D presented at the lower 2θ region, which are assigned as the layered perovskite with n equals to 4, 3, 2 and 1, respectively. The experimental XRD peaks and $d_{(100)}$ values of these layered structures are also compared to the simulated values and the result is in good agreement with each other. The simulated XRD of layered perovskite is presented in Figure S2 (Supporting Information) and the comparison is summarized in Table S1 (Supporting

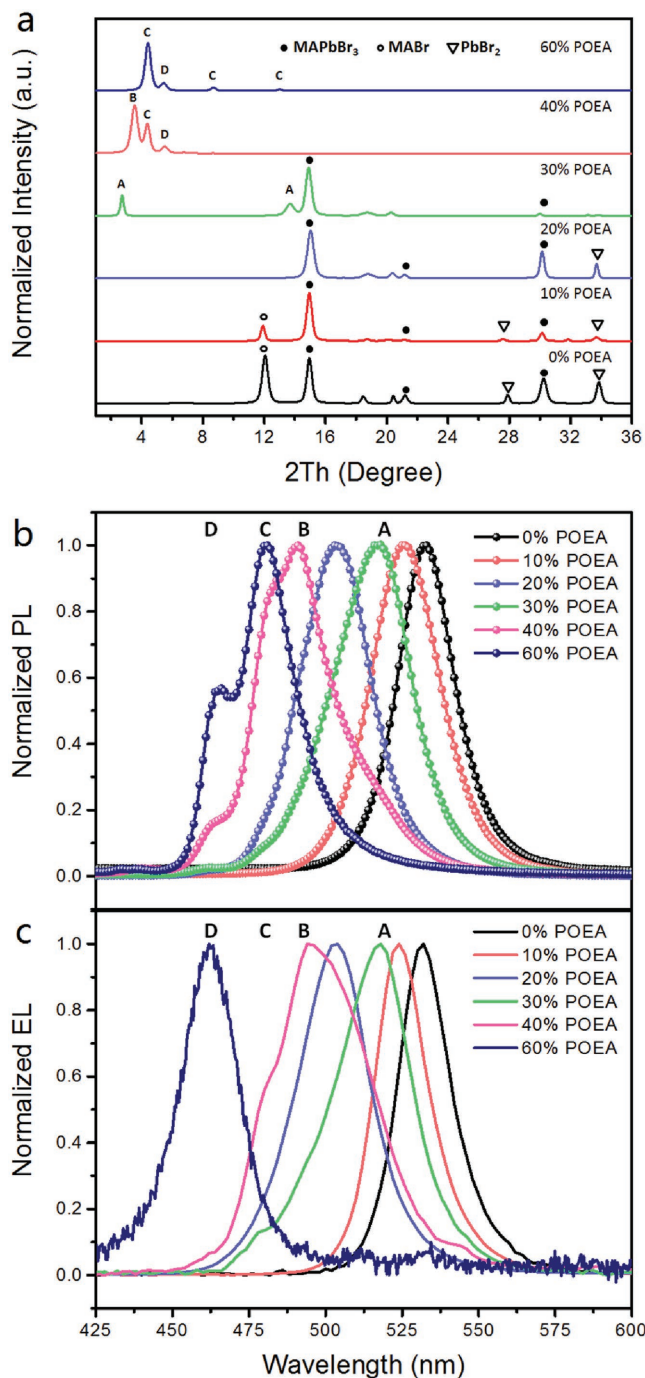


Figure 2. a) XRD pattern and b) PL spectra of perovskite thin films fabricated from $\text{CH}_3\text{NH}_3\text{PbBr}_3$ precursor solutions with different ratio of POEA. The XRD peak of MABr at around 12° is in agreement with previous report.^[49] c) EL spectra of perovskite LED devices with different ratio of POEA. The labels A, B, C, and D in panels (b) and (c) correspond to the emission peaks of layered perovskites with different n values.

Information). The 30% POEA doped perovskite film discussed above mainly composed of layer with $n = 4$. The film doped with 40% POEA composed of layers with $n = 1, 2$ and 3 while further increasing the doping to 60% resulted in layered perovskite film with $n = 1$ and 2 . It is worth to note that the formation

of layered perovskite with multiple n values is commonly observed, it is difficult to obtain pure layered-structure single crystal even using precisely controlled synthetic method.^[18] Nevertheless, the multiple layered perovskite films prepared by our simple solution processing method show good film quality with high coverage and relatively large grain size of over $1 \mu\text{m}$ and they are readily to be used for emission study in devices.

The relationship between the emission properties and the perovskite film structures were studied using both PL and EL studies. The PL spectra of the films are shown in Figure 2b. In general, when the films changed from bulk to layered structure, the emission blueshifted accordingly. The PL peak of pristine $\text{CH}_3\text{NH}_3\text{PbBr}_3$ film is located at 532 nm, which is in agreement with other reported value.^[26] When 10% of POEA was added, the PL peak slightly blueshifted to 524 nm. As the shape and size of the perovskite crystals are comparable to those in the pristine film, the spectral shift is unlikely due to the effect of structure change, instead, we attribute the shift to the interaction between the amine group of POEA and the surface of the perovskite, which resulted in surface trap passivation effect and led to the blueshift of the spectrum.^[50] This effect was also observed in other hybrid systems when amine functionalized polymer was in contact with the perovskite surface.^[51] While 20% POEA was added, a pure $\text{CH}_3\text{NH}_3\text{PbBr}_3$ phase with rod-like crystals was achieved. This change of crystal shape resulted in a significant blueshift of the emission spectrum with peak at 504 nm. It is worth to note that the pristine, 10%- and 20%-POEA doped perovskites all showed uniform Gaussian emission spectra, indicated that the emission was originated from pure phase. However, upon further doping, multiple emission peaks were observed. In the case of 30%-POEA doped film, both bulk and layered structures were existed. The corresponding emission spectrum showed a main peak at ≈ 520 nm with a non-Gaussian distribution. Deconvoluted spectrum, as shown in Figure S3a (Supporting Information), reveals that indeed there is another emission peak located at $\approx 506 \pm 2$ nm, which corresponds to the emission from the rod-like crystals. While the emission peak at 520 ± 2 nm is from the layered structure A ($n = 4$), which appears as large grains in the SEM image in Figure 1a.

In the case of the 40%-POEA doped film, as several types of layer structures are coexisted, the PL spectrum is much more complicated. The resolved PL spectrum shows four individual peaks of 508 ± 2 , 492 ± 2 , 480 ± 2 and 462 ± 2 nm (Figure S3c, Supporting Information), which are originated from the rod-like crystal and layered structures with $n = 3, 2$ and 1 , respectively. In the 60%-POEA doped case, the PL spectrum can be resolved into two emissions with peaks at 480 ± 2 and 464 ± 2 nm (Figure S3d, Supporting Information), which suggested that only layered structures of $n = 2$ and 1 are existed and the result is in good agreement with the XRD study. It is worth to note that the bandgap and emission peak of 2D inorganic-organic perovskite materials are mainly determined by the bonding length and angle between the Br and Pb atoms in the inorganic part. These parameters indeed are affected by the choice of the organic ligands in the hybrid system.^[52,53] According to previous studies, through the modulation of the chemical structure of the organic ligands, the PL emission of the $n = 1$ Pb and Br-based layered perovskites could be altered

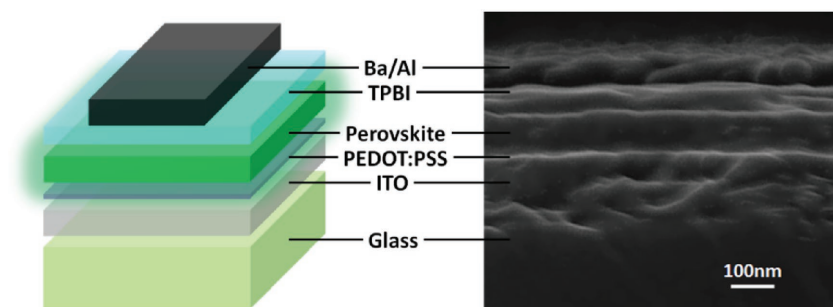


Figure 3. Device configuration and SEM cross section of LED device in the structure of Glass/ITO/PEDOT:PSS/Perovskite(30% POEA-doping)/TPBI/Ba/Al.

from 400 to 540 nm.^[54,55] However, despite the strong dependency of the bandgap on the choice of organic ligand, it is generally observed that upon decreasing the layer value n , the bandgap of the layered perovskite structure increases due to the quantum confinement effect.^[18,56]

EL study was performed using LEDs with structure of ITO/PEDOT:PSS(30 nm)/Perovskite(80 nm)/TPBI(50 nm)/Ba(4 nm)/Al(100 nm) as depicted in **Figure 3**. According to **Figure 2c**, the EL spectra of the perovskite LED devices are nearly the same as the PL spectra in all the cases in terms of emission peak positions and a summary of the emission peaks from both PL and EL are shown in **Table 1**. However, the EL spectra of the perovskite films with multiple n layers, such as the cases of 40%- and 60%-POEA doped films, are quite different from their PL spectra in terms of the shape of the spectrum. The EL of 40%-POEA doped device also can be deconvoluted into multiple emission spectra with peaks at 480 ± 2 , 494 ± 2 , and 508 ± 2 nm (**Figure S3b**, Supporting Information) but the emission intensity of each peak is different to that in the PL spectrum. This is probably due to the different recombination mechanism between the photoexcited film and electrically driven device. The emission peak of the 60%-POEA device is located at 462 nm, which is corresponding to the emission from layered perovskite with $n = 1$.

The light emitting performance of the perovskite LEDs is also summarized in **Table 1** and their corresponding current density and luminance versus voltage characteristics and EQE are shown in **Figure 4a,b**, respectively. The highest luminance of 2146.1 cd m^{-2} was achieved in the 10%-POEA doped devices at relatively high J of 213 mA cm^{-2} and V of 6.4 V, which indeed led to low EQE and CE. Higher EQE and CE were achieved

Table 1. Perovskite LED properties with different ratio of POEA. The EL and PL spectra could be divided into several peaks in the case of 30, 40, and 60% POEA with 2 nm deviation.

POEA Ratio	Max. L [cd m^{-2}]	Max. EQE [%]	Max. CE [cd A^{-1}]	EL Peak [nm]	PL Peak [nm]
0%	105.88	0.06	0.24	532	532
10%	2146.11	0.31	1.21	524	524
20%	138.06	2.76	5.92	504	504
30%	64.20	2.82	8.23	506, 520	506, 520
40%	19.25	1.1	2.1	480, 494, 508	462, 480, 492, 508
60%	1.26	0.06	0.07	462	464, 480

when further increasing the doping content and maximized at the 30%-POEA doped devices with best EQE and CE reaching 2.82% and 8.23 cd A^{-1} , respectively. Further increasing the doping content resulted in a drop of device performance. The reproducibility of devices is presented in **Figure S4** (Supporting Information). It is worth to note that the emission color of the devices slowly shifted from green to bluish-green and finally to blue upon increasing the doping content. The corresponding color coordinates of the perovskite LED devices are plotted in the CIE chromaticity diagram as shown in **Figure 5a**

for a clear illustration of their emitting colors. We also compare the device performance in this work to those in other reports by summarizing the maximized EQE at a specific luminescence and emission color (**Figure 5b**). It shows that our devices can reach relatively high luminance and EQE when compares to other devices. It is also worth to note that an encouraging EQE of over 1% was achieved for perovskite LED emitting sky blue color, which represents a significant progress in blue emitting perovskite devices.

To correlate the light emitting properties to the perovskite film structures, we further analyzed the J - V , L - V , and the EQE curves of the devices. According to the J - V curve shown in **Figure 4a**, perovskite LED devices suffered from an obvious leakage current in low POEA doping cases and the leakage current was suppressed when the concentration of POEA increased. The large leakage current is attributed to the relatively poor coverage of the perovskite film and the existence of large number of pinholes, which led to direct contact between poly(3,4-ethylenedioxythiophene):poly(styrene sulfonate) (PEDOT:PSS) and TPBI. Increasing the concentration of POEA can reduce the number of pinholes and improve the coverage of the perovskite film, as observed in the SEM and atomic force microscopy (AFM) images in **Figure 1a** and **Figure S5** (Supporting Information), respectively, resulting in a decrease of leakage current in perovskite LED devices. According to the L - V and EQE curves, the pristine $\text{CH}_3\text{NH}_3\text{PbBr}_3$ -based devices were easily broken down and shown poor stability at high voltage due to the undesired morphology and the presence of large amount of impure MABr phase in the $\text{CH}_3\text{NH}_3\text{PbBr}_3$ film. While 10% POEA was added, the devices still present a high leakage current due to poor film coverage. However, as a purer $\text{CH}_3\text{NH}_3\text{PbBr}_3$ phase was obtained, current injection became easier and led to an overall high current density. In addition, the amine group of POEA could passivate the surface of $\text{CH}_3\text{NH}_3\text{PbBr}_3$ as evidenced by the blueshift of emission spectrum and supported by other report,^[50] this contributed to a higher luminance and EQE of the LED devices. Moreover, the EL spectrum showed a much improved stability at different applied voltage and current density (**Figure S6**, Supporting Information), which suggests that previously observed poor EL stability at increased applied voltage for perovskite LEDs may be related to surface defects.^[57,58] In the 20% POEA-doped case, a high EQE of over 2.7% was obtained at $\approx 4 \text{ V}$. We attribute the improvement to the reduced leakage current and also to the high purity $\text{CH}_3\text{NH}_3\text{PbBr}_3$ phase with increased crystallinity

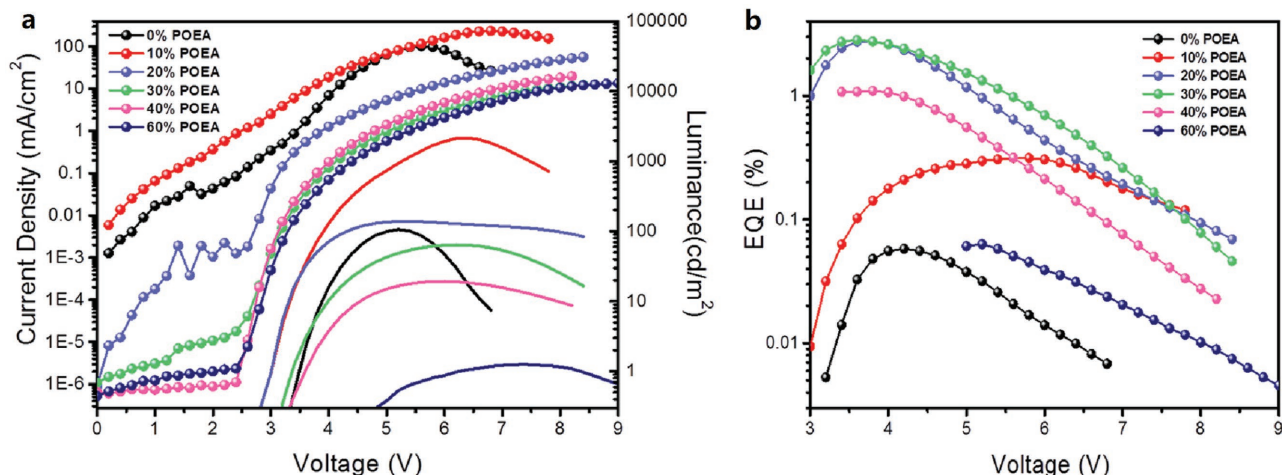


Figure 4. a) Current density and luminance versus voltage characteristics of perovskite LEDs doped with different ratio of POEA. The solid lines and lines with dot correspond to luminance and current density, respectively. b) EQE versus voltage characteristic of perovskite LEDs with different ratio of POEA.

and lower defect concentration. However, we also observed that the overall current density and luminance were lower than the 10% POEA-doped case probably due to the increased content of the insulating POEA molecules. The highest EQE of 2.82% and CE of 8.23 cd A⁻¹ were obtained in the 30% POEA-doped device with a significant reduced leakage current due to the improved coverage of the film. The presence of layered structure was accounted for the improved coverage but with a tradeoff it reduced the overall current density in the devices. The current density further decreased upon increasing POEA doping to 40% and 60% in the layered perovskite films. The maximum EQE of the corresponding devices reduces to 1.1% and 0.06%, respectively. Nevertheless, these EQE values are among the best reported ones for blue emitting devices as summarized in Figure 5b.

In order to further understand how the POEA affects the LED device performance and the appearance of EQE roll-off in

our perovskite LEDs, which is also commonly observed in other perovskite-based LEDs, PL lifetime and time-resolved pump-probe measurements were performed on the perovskite films. All the measurements were acquired by femtosecond pulsed laser at a central wavelength of 345 nm with a repetition rate of 1 kHz as the excitation source. **Figure 6a** shows the PL lifetime of perovskite films with different concentration of POEA. With increasing POEA concentration from 0% to 30%, the PL lifetime continues to increase, suggesting the POEA may provide an efficient surface passivation effect and reduced the trap-assisted recombination.^[59,60] However, the PL lifetime started to drop when pure layered structure was formed in the 40% and 60% POEA case. The decreased lifetime could be attributed to the increase exciton binding energy in the layered structure when the organic POEA with low dielectric constant becomes a major component in the film.^[61,62] As the best performance and the longest PL lifetime were achieved in the 30% POEA-doped

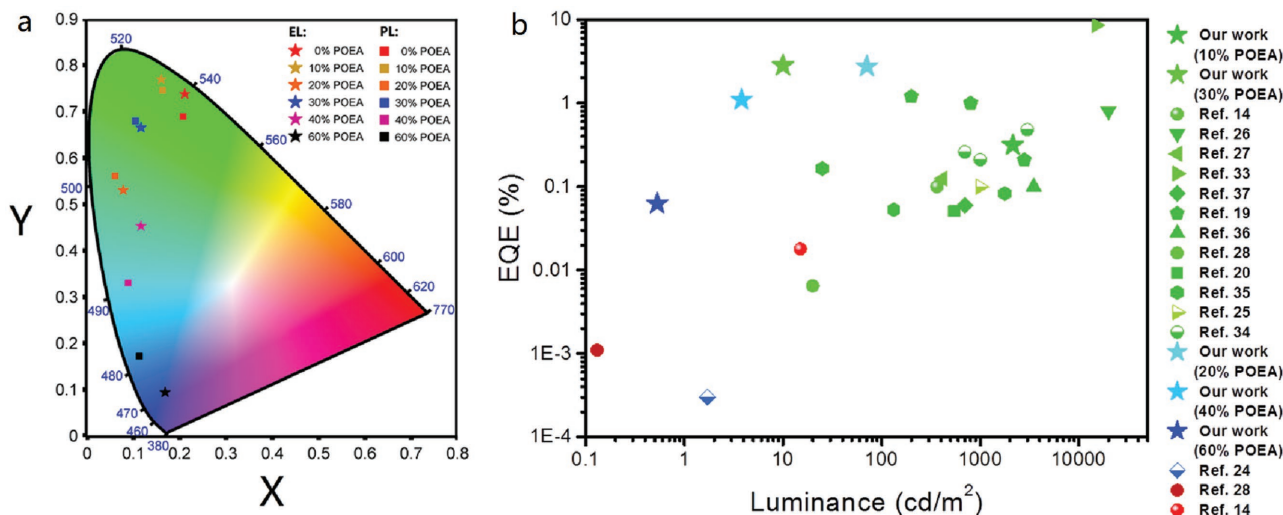


Figure 5. a) Color coordinates of the EL of perovskite LEDs and PL of perovskite films plotted in the CIE chromaticity diagram. b) Comparison of the performance of perovskite LEDs from our work and published results, the color of the symbols mimics the actual emission color of the LEDs.

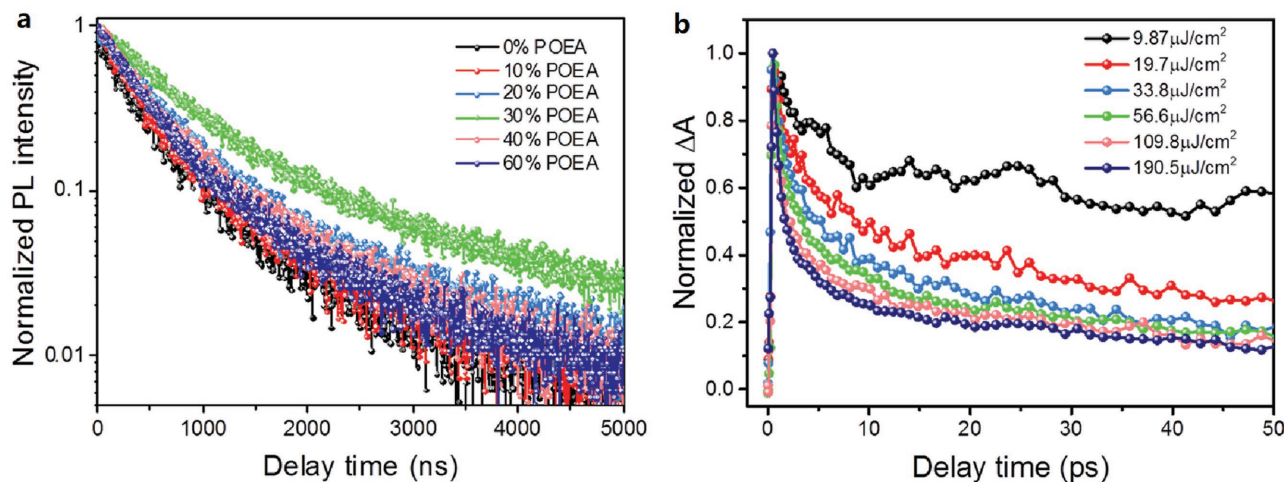


Figure 6. a) PL lifetime traced at the emission peak of perovskite films doped with different ratio of POEA under a fixed excitation fluence of $1 \mu\text{J}/\text{cm}^2$. b) Transient absorption kinetics probed at 755 nm on perovskite film under different pump fluences in the 30% POEA case. The excitation wavelength for both pump-probe and PL lifetime measurements is 345 nm.

samples, we therefore further studied the kinetics of charge recombination using transient absorption experiment. The transient absorption spectrum of the perovskite film pumped at 345 nm is shown in Figure S7 (Supporting Information). The largest $\Delta T/T$ signal was shown at 755 nm, which corresponds to the excited state absorption of the perovskite film. We therefore tracked the transient absorption kinetics at 755 nm with different excitation fluences and we observed that the carrier kinetic was strongly dependent on the excitation fluence, as shown in Figure 6b. The result showed that the carrier lifetime is decreased with increasing the pump pulse fluence. Such phenomenon can be explained by the strong Auger recombination in the films, which happens when the energy from the relaxation of an excited state to its ground state is consumed to promote an electron in another excited state to higher energy states and therefore reduces the chance for radiative relaxation. The Auger recombination became dominated at high density of electron in excited states due to the increase of excitation fluence in our case, which made Auger recombination become one of the possible reasons resulting in the EQE roll-off in the devices. Such a phenomenon was also observed in many other perovskite-based films and our study is in good agreement with other reports.^[63,64] Therefore the development of new strategies to suppress the Auger recombination and trap-assisted recombination will be critical to further improve perovskite LED properties in future study.

In summary, by introducing an amine-based small molecule, POEA, which can strongly interact with the $\text{CH}_3\text{NH}_3\text{PbBr}_3$ perovskite, to the precursor solution, we demonstrated that the structure of the resulted organic-inorganic perovskite films could be systematically tuned from bulk to layered structure. The structure-property relationship of the hybrid perovskite films were studied through a combination of experiments including PL emission, PL lifetime and transient absorption to study the optical properties and XRD, SEM and AFM study for structural and morphological characterization. It was found that with increasing doping content of the small molecule, the perovskite films started to grow from cubic to rod-like crystals

and eventually formed the 2D layered films. This structural modulation led to a significant change in optical property of the films and a hypsochromic shift of emission from green to blue was obtained upon increasing doping content of the molecules. LEDs based on the perovskite films were fabricated to evaluate their light emitting properties. By adding appropriate ratio of POEA, the device performance and spectrum stability could significantly improve with the best EQE reaching over 2.8% and CE over 8.2 cd A^{-1} resulted from the improved film coverage and surface trap passivation effect induced by the POEA. At high doping ratios, layered perovskite structure with significant blueshifted emission was obtained. As a result, we also demonstrated blue emitting perovskite LEDs, which were rarely reported due to the intrinsic difficulty in obtaining high quality large bandgap perovskite film. Despite these encouraging results, the perovskite LEDs still suffered from severe efficiency roll-off problem, which is probably induced by strong Auger recombination as suggested by the transient absorption kinetics study. We believe that our study demonstrated an effective means to tune the film structure and optical property of hybrid perovskite materials, and the successful application of the hybrid films for making high-performance LEDs also suggested that this class of material has great potential for future application in other functional devices.

Experimental Section

Perovskite Precursor: 0.1 mmol PbBr_2 and 0.3 mmol MABr and appropriate amount of POEA were dissolved in 1 mL DMF to form a 0.1 M perovskite precursor solution with different ratio of POEA. The ratio of x% POEA means $m_{\text{POEA}}/(1/3m_{\text{MABr}} + m_{\text{PbBr}_2}) = x\%$. The precursor solution was stirred for 2 d without any heating.

Perovskite LED Device Fabrication: ITO-coated glass substrates were cleaned by sonication in detergent, acetone, deionized water, and isopropyl alcohol subsequently. After 4 min oxygen plasma treatment, diluted PEDOT:PSS (Clevios, CH8000) was spin-coated above ITO-coated glass substrate at 3500 rpm for 30 s and annealed at 120°C for 20 min in ambient. Then 0.1 M perovskite precursor solution was spin-coated on PEDOT:PSS film in the spin-coat speed of 4000 rpm for

50 s and annealed at 100 °C for 30 min in humidity of 15%. A 50 nm thick TPBI was evaporated to cover perovskite layer, followed by the deposition of Ba(4 nm) and Al(100 nm) through thermal deposition in high vacuum condition.

Perovskite Film Characterization: SEM (ZEISS Merlin) measurement was carried based on the structure of ITO/PEDOT:PSS/Perovskite. XRD measurement was carried based on the structure of Glass/PEDOT:PSS/Perovskite by an X-ray diffractometer (PANalytical X'pert PRO) equipped with Cu-K α X-ray tube. PL spectra were measured by a spectrofluorometer (Perkin-Elmer LS 55).

Transient Absorption and Pump-Probe Measurements: Time-resolved transient absorption and pump-probe measurements were performed on perovskite films by using a Ti:sapphire oscillator seeded regenerative amplifier (Spectra Physics, Spitfire Ace), which gives an output with a pulse energy of 2.0 mJ at 800 nm and a repetition rate of 1 kHz. The 800 nm laser beam was split into two portions. The larger portion of the beam passed through an optical parametric amplifier (Spectra Physics, TOPAS-Prime) to generate the 345 nm pump beam by fourth harmonic generation of signal at 1380 nm. The small portion of the 800 nm beam was focused onto a 1 mm sapphire plate to generate white light continuum. The white light beam was split into two beams, one as the probe and the other as the reference to correct the pulse-to-pulse intensity fluctuations. The intensities of signal and reference beams were measured by photodiodes that are connected to lock-in amplifiers and the computer. The pump beam was focused onto the sample with a beam size of 300 μ m and overlaps with the smaller-diameter (100 μ m) probe beam. The delay between the pump and probe pulses was varied by a computer-controlled translation stage (Newport, ESP 300). The pump beam was modulated by an optical chopper at a frequency of 500 Hz. The variation transmittance at selected probe wavelength by monochromator (Princeton Instruments, Acton SP2150i) is recorded as a function of time delay between pump and probe pulses. All the experiments were performed at room temperature.

Photoluminescence Lifetime Measurement: PL of samples were measured by using an output at a central wavelength of 345 nm with pulse duration of 120 fs and a repetition rate of 1 kHz as the excitation source, which is generated from an optical parametric amplifier (TOPAS-Prime) pumped by a mode-locked Ti:sapphire oscillator seeded regenerative amplifier (SpectraPhysics Spitfire Ace). The laser beam was focused onto the samples using a lens with a focus length of 100 mm. The emission was collected at the direction perpendicular to the excitation beam to minimize the scattering. The emission signal was directed into a monochromator with two exit ports (Princeton Instruments, Acton 2300i). One port is integrated with CCD (Princeton Instruments, Pixis 100B) for spectra measurement. The other port is mounted with a photon counting detector combined with the multichannel scaler/averager SR430 for time-resolved emission measurement. A 360 nm long pass filter was placed before the spectrometer to minimize the scattering from the excitation light.

Perovskite LED Device Characterization: Current density–voltage–radiance measurement was carried by a Keithley 2400 source measurement unit and a calibrated silicon photodiode. The EL spectrum was obtained by an optical analyzer, Photo Research PR705, while the emission of the 60%-POEA device was recorded by MayaPro 2000 with an optical fiber from Ocean Optics. The external quantum efficiency values were calculated assuming a Lambertian emission profile.

Simulation of XRD Patterns of Layered Structures: The calculations were based on the layer-perovskites models from $n = 1$ to $n = 4$, which contained Pb-I $_6$ octahedral units and a middle stacking region with different amounts of POEA. For instance, $n = 1$ layer structure contained 45 atoms and its lattice constant along the z-direction was set to 16.42 Å, same with the experimental data. The relaxation calculations were performed using Vienna ab initio simulation package code with the standard frozen-core projector augmented-wave method. Atoms were relaxed until the Hellmann–Feynman forces on them were below 0.05 eV Å $^{-1}$. After the relaxation, the Powder Diffraction Simulation of Material Studio to simulate the XRD plots was employed. Here, the copper source was chosen to get the final XRD simulating images of the

relaxed layer models. The range of incident angle was from 1° to 36°, in comparison with the experimental one. It was found that the main peaks were consistent with each other very well.

Supporting Information

Supporting Information is available from the Wiley Online Library or from the author.

Acknowledgements

The work was financially supported by the Ministry of Science and Technology (No. 2014CB643505) and the Natural Science Foundation of China (Nos. 51323003, 51573057, 51573059, and 11574088).

Received: June 15, 2016

Revised: November 9, 2016

Published online: December 21, 2016

- [1] S. D. Stranks, G. E. Eperon, G. Grancini, C. Menelaou, M. J. P. Alcocer, T. Leijtens, L. M. Herz, A. Petrozza, H. J. Snaith, *Science* **2013**, *342*, 341.
- [2] G.-C. Xing, N. Mathews, S.-Y. Sun, S. S. Lim, Y. M. Lam, M. Grätzel, S. Mhaisalkar, T. C. Sum, *Science* **2013**, *342*, 344.
- [3] H. J. Snaith, *J. Phys. Chem. Lett.* **2013**, *4*, 3623.
- [4] G. E. Eperon, S. D. Stranks, C. Menelaou, M. B. Johnston, L. M. Herz, H. J. Snaith, *Energy Environ. Sci.* **2014**, *7*, 982.
- [5] W.-J. Yin, H.-Y. Chen, T.-T. Shi, S.-H. Wei, Y.-F. Yan, *Adv. Electron. Mater.* **2015**, *1*, 1500044.
- [6] H. Kim, K.-G. Lim, T.-W. Lee, *Energy Environ. Sci.* **2016**, *9*, 12.
- [7] K.-G. Lim, S. Ahn, H. Kim, M.-R. Choi, D. H. Huh, T.-W. Lee, *Adv. Mater. Interfaces* **2016**, *3*, 1500678.
- [8] K.-G. Lim, H.-B. Kim, J. Jeong, H. Kim, J. Y. Kim, T.-W. Lee, *Adv. Mater.* **2014**, *26*, 6461.
- [9] C.-Y. Yi, J.-S. Luo, S. Meloni, A. Boziki, N. Ashari-Astani, C. Grätzel, S. M. Zakeeruddin, U. Röthlisberger, M. Grätzel, *Energy Environ. Sci.* **2016**, *9*, 656.
- [10] S.-Y. Hsiao, H.-L. Lin, W.-H. Lee, W.-L. Tsai, K.-M. Chiang, W.-Y. Liao, C.-Z. Ren-Wu, C.-Y. Chen, H.-W. Lin, *Adv. Mater.* **2016**, *28*, 7013.
- [11] W. S. Yang, J. H. Noh, N. J. Jeon, Y. C. Kim, S. Ryu, J. Seo, S. I. Seok, *Science* **2015**, *348*, 1234.
- [12] C.-Y. Yi, X. Li, J.-S. Luo, S. M. Zakeeruddin, M. Grätzel, *Adv. Mater.* **2016**, *28*, 2964.
- [13] T. J. Jacobsson, J.-P. Correa-Baena, M. Pazoki, M. Saliba, K. Schenk, M. Grätzel, A. Hagfeldt, *Energy Environ. Sci.* **2016**, *9*, 1706.
- [14] Z.-K. Tan, R. S. Moghaddam, M. L. Lai, P. Docampo, R. Higler, F. Deschler, M. Price, A. Sadhanala, L. M. Pazos, D. Credgington, F. Hanusch, T. Bein, H. J. Snaith, R. H. Friend, *Nat. Nanotechnol.* **2014**, *9*, 687.
- [15] F. Zhang, H.-Z. Zhong, C. Chen, X.-G. Wu, X.-M. Hu, H.-L. Huang, J.-B. Han, B.-S. Zou, Y.-P. Dong, *ACS Nano* **2015**, *9*, 4533.
- [16] L. C. Schmidt, A. Pertegás, S. González-Carrero, O. Malinkiewicz, S. Agouram, G. M. Espallargas, H. J. Bolink, R. E. Galian, J. Pérez-Prieto, *J. Am. Chem. Soc.* **2014**, *136*, 850.
- [17] M. F. Aygüler, M. D. Weber, B. M. D. Puscher, D. D. Medina, P. Docampo, R. D. Costa, *J. Phys. Chem. C* **2015**, *119*, 12047.
- [18] J. A. Sichert, Y. Tong, N. Mutz, M. Vollmer, S. Fischer, K. Z. Milowska, R. G. Cortadella, B. Nickel, C. Cardenas-Daw, J. K. Stolarczyk, A. S. Urban, J. Feldmann, *Nano Lett.* **2015**, *15*, 6521.
- [19] G.-R. Li, Z.-K. Tan, D.-W. Di, M. L. Lai, L. Jiang, J. H.-W. Lim, R. H. Friend, N. C. Greenham, *Nano Lett.* **2015**, *15*, 2640.

- [20] J. C. Yu, D. B. Kim, G. Baek, B. R. Lee, E. D. Jung, S. Lee, J. H. Chu, D.-K. Lee, K. J. Choi, S. Cho, M. H. Song, *Adv. Mater.* **2015**, *27*, 3492.
- [21] R. L. Z. Hoye, M. R. Chua, K. P. Musselman, G.-R. Li, M.-L. Lai, Z.-K. Tan, N. C. Greenham, J. L. MacManus-Driscoll, R. H. Friend, D. Credgington, *Adv. Mater.* **2015**, *27*, 1414.
- [22] A. Sadhanala, A. Kumar, S. Pathak, A. Rao, U. Steiner, N. C. Greenham, H. J. Snaith, R. H. Friend, *Adv. Electron. Mater.* **2015**, *1*, 1500008.
- [23] O. A. Jaramillo-Quintero, R. S. Sanchez, M. Rincon, I. Mora-Sero, *J. Phys. Chem. Lett.* **2015**, *6*, 1883.
- [24] N. K. Kumawat, A. Dey, A. Kumar, S. P. Gopinathan, K. L. Narasimhan, D. Kabra, *ACS Appl. Mater. Inter.* **2015**, *7*, 13119.
- [25] A. Sadhanala, S. Ahmad, B.-D. Zhao, N. Giesbrecht, P. M. Pearce, F. Deschler, R. L. Z. Hoye, K. C. Gödel, T. Bein, P. Docampo, S. E. Dutton, M. F. L. D. Volder, R. H. Friend, *Nano Lett.* **2015**, *15*, 6095.
- [26] J.-P. Wang, N.-N. Wang, Y.-Z. Jin, J.-J. Si, Z.-K. Tan, H. Du, L. Cheng, X.-L. Dai, S. Bai, H.-P. He, Z.-Z. Ye, M. L. Lai, R. H. Friend, W. Huang, *Adv. Mater.* **2015**, *27*, 2311.
- [27] Y.-H. Kim, H. Cho, J. H. Heo, T.-S. Kim, N. Myoung, C.-L. Lee, S. H. Im, T.-W. Lee, *Adv. Mater.* **2015**, *27*, 1248.
- [28] N. K. Kumawat, A. Dey, K. L. Narasimhan, D. Kabra, *ACS Photonics* **2015**, *2*, 349.
- [29] G.-C. Xing, N. Mathews, S. S. Lim, N. Yantara, X.-F. Liu, D. Sabba, M. Grätzel, S. Mhaisalkar, T. C. Sum, *Nat. Mater.* **2014**, *13*, 476.
- [30] J. Xing, X. F. Liu, Q. Zhang, S. T. Ha, Y. W. Yuan, C. Shen, T. C. Sum, Q.-H. Xiong, *Nano Lett.* **2015**, *15*, 4571.
- [31] H.-M. Zhu, Y.-P. Fu, F. Meng, X.-X. Wu, Z.-Z. Gong, Q. Ding, M. V. Gustafsson, M. T. Trinh, S. Jin, X.-Y. Zhu, *Nat. Mater.* **2015**, *14*, 636.
- [32] F. Deschler, M. Price, S. Pathak, L. E. Klintberg, D.-D. Jarausch, R. Higler, S. Hüttner, T. Leijtens, S. D. Stranks, H. J. Snaith, M. Atatüre, R. T. Phillips, R. H. Friend, *J. Phys. Chem. Lett.* **2014**, *5*, 1421.
- [33] H. Cho, S.-H. Jeong, M.-H. Park, Y.-H. Kim, C. Wolf, C.-L. Lee, J. H. Heo, A. Sadhanala, N. Myoung, S. Yoo, S. H. Im, R. H. Friend, T.-W. Lee, *Science* **2015**, *350*, 1222.
- [34] Y.-C. Ling, Z. Yuan, Y. Tian, X. Wang, J. C. Wang, Y. Xin, K. Hanson, B.-W. Ma, H.-W. Gao, *Adv. Mater.* **2016**, *28*, 305.
- [35] J.-Q. Li, S. G. R. Bade, X. Shan, Z.-B. Yu, *Adv. Mater.* **2015**, *27*, 5196.
- [36] J. C. Yu, D. B. Kim, E. D. Jung, B. R. Lee, M. H. Song, *Nanoscale* **2016**, *8*, 7036.
- [37] X. Qin, H.-L. Dong, W.-P. Hu, *Sci. China Mater.* **2015**, *58*, 186.
- [38] M. Era, S. Morimoto, T. Tsutsui, S. Saito, *Appl. Phys. Lett.* **1994**, *65*, 676.
- [39] T. Hattori, T. Taira, M. Era, T. Tsutsui, S. Saito, *Chem. Phys. Lett.* **1996**, *254*, 103.
- [40] M. Coelle, W. Brueetting, M. Schwoerer, M. Yahiro, T. Tsutsui, *Proc. SPIE* **2001**, *4105*, 328.
- [41] M. Era, S. Morimoto, T. Tsutsui, S. Saito, *Synth. Met.* **1995**, *71*, 2013.
- [42] J. Byun, H. Cho, C. Wolf, M. Jang, A. Sadhanala, R. H. Friend, H. Yang, T.-W. Lee, *Adv. Mater.* **2016**, *28*, 7515.
- [43] D. Liang, Y.-L. Peng, Y.-P. Fu, M. J. Shearer, J.-J. Zhang, J.-Y. Zhai, Y. Zhang, R. J. Hamers, T. L. Andrew, S. Jin, *ACS Nano* **2016**, *10*, 6897.
- [44] M.-J. Yuan, L. N. Quan, R. Comin, G. Walters, R. Sabatini, O. Voznyy, S. Hoogland, Y.-B. Zhao, E. M. Beauregard, P. Kanjanaboos, Z.-H. Lu, D. H. Kim, E. H. Sargent, *Nat. Nanotechnol.* **2016**, *11*, 872.
- [45] Y.-N. Xia, P.-D. Yang, Y.-G. Sun, Y.-Y. Wu, B. Mayers, B. Gates, Y.-D. Yin, F. Kim, H.-Q. Yan, *Adv. Mater.* **2003**, *15*, 353.
- [46] D. B. Mitzi, M. T. Prikas, K. Chondroudis, *Chem. Mater.* **1999**, *11*, 542.
- [47] D. B. Mitzi, D. R. Medeiros, P. R. L. Malenfant, *Inorg. Chem.* **2002**, *41*, 2134.
- [48] Z.-Y. Cheng, J. Lin, *CrystEngComm* **2010**, *12*, 2646.
- [49] J. H. Heo, D. H. Song, S. H. Im, *Adv. Mater.* **2014**, *26*, 8179.
- [50] Y.-C. Shao, Z.-G. Xiao, C. Bi, Y.-B. Yuan, J.-S. Huang, *Nat. Commun.* **2014**, *5*, 5784.
- [51] C. Sun, Z.-H. Wu, H.-L. Yip, H. Zhang, X.-F. Jiang, Q.-F. Xue, Z.-C. Hu, Z.-H. Hu, Y. Shen, M.-K. Wang, F. Huang, Y. Cao, *Adv. Energy Mater.* **2016**, *6*, 1501534.
- [52] Z. T. Xu, D. B. Mitzi, C. D. Dimitrakopoulos, K. R. Maxcy, *Inorg. Chem.* **2003**, *42*, 2031.
- [53] D. B. Mitzi, C. D. Dimitrakopoulos, L. L. Kosbar, *Chem. Mater.* **2001**, *13*, 3728.
- [54] Y. Tabuchi, K. Asai, M. Rikukawa, K. Sanui, K. Ishigure, *J. Phys. Chem. Solids* **2000**, *61*, 837.
- [55] D. B. Mitzi, K. Chondroudis, C. R. Kagan, *Inorg. Chem.* **1999**, *38*, 6246.
- [56] A. M. Smith, S.-M. Nie, *Acc. Chem. Res.* **2010**, *43*, 190.
- [57] X.-Y. Zhang, H. Lin, H. Huang, C. Reckmeier, Y. Zhang, W. C. H. Choy, A. L. Rogach, *Nano Lett.* **2016**, *16*, 1415.
- [58] A. Sadhanala, A. Kumar, S. Pathak, A. Rao, U. Steiner, N. C. Greenham, H. J. Snaith, R. H. Friend, *Adv. Electron. Mater.* **2015**, *1*, 1500008.
- [59] N. K. Noel, A. Abate, S. D. Stranks, E. S. Parrott, V. M. Burlakov, A. Goriely, H. J. Snaith, *ACS Nano* **2014**, *8*, 9815.
- [60] A. Ng, Z.-W. Ren, Q. Shen, S. H. Cheung, H. C. Gokkaya, G.-X. Bai, J.-C. Wang, L.-J. Yang, S. K. So, A. B. Djurišić, W. W.-F. Leung, J.-H. Hao, W. K. Chan, C. Surya, *J. Mater. Chem. A* **2015**, *3*, 9223.
- [61] T. Fujitaa, H. Nakashimaa, M. Hirasawab, T. Ishihara, *J. Lumin.* **2000**, *87–89*, 847.
- [62] X. Hong, T. Ishihara, A. V. Nurmikko, *Phys. Rev. B* **1992**, *45*, 6961.
- [63] J. S. Manser, P. V. Kamat, *Nat. Photonics* **2014**, *8*, 737.
- [64] C. Wehrenfennig, M.-Z. Liu, H. J. Snaith, M. B. Johnston, L. M. Herz, *Energy Environ. Sci.* **2014**, *7*, 2269.